

Electrochemical Behavior of a Z2CND18-12N Stainless Steel in High Temperature and High Pressure Water Containing H₃BO₃, LiOH and Chloride Ions

Kewei Fang*, Li Wang, Kunjie Luo and Chengtao Li

Suzhou Nuclear Power Research Institute, Suzhou 215004, China

*E-mail: fangkewei@cgnpc.com.cn

Received: 15 March 2022 / Accepted: 4 May 2022 / Published: 6 June 2022

The effect of Cl⁻ on the electrochemical behavior of a Z2CND18-12N stainless steel (SS) in H₃BO₃-LiOH high temperature high pressure water was studied using the measurements of potentiodynamic polarization curve, electrochemical impedance spectroscopy (EIS) and current-time transient curve. The results indicated that the Z2CND18-12N SS exhibited anodic passivation behavior in the tested solutions. When Cl⁻ was added to the tested solution, the corrosion potential had a positive shift with an acceleration of corrosion rate, making the passive regions unstable and shrinking. At the same applied potential, the corrosion film formed on the surface of the Z2CND18-12N SS in B-Li water containing 10ppm and 100ppm Cl⁻ at 290°C became relatively looser and contained more defects compared to that without Cl⁻ addition, which accounted for the instability of passive film, the shrinking of passive regions and the acceleration of corrosion process.

Keywords: Z2CND18-12N stainless steel; H₃BO₃-LiOH high temperature water; Cl⁻, Electrochemical behaviors

1. INTRODUCTION

Z2CND18-12N austenitic stainless steel (SS), which was developed in France during 1970s, has been widely used in pressurized water reactor (PWR) nuclear power plant owing to its excellent corrosion performance[1]. Previous studies showed that SSs were sensitive to stress corrosion cracking in high temperature water environments containing H₃BO₃ and LiOH(B-Li), especially when Cl⁻ was present[2-5]. Féron[2] and Li[5] shown that Cl⁻ will increase the susceptibility of stainless steel SCC and IASCC, and Ehrnsten[3] and Calvar[4] believe that Cl⁻ can damage the integrity of the oxide film, thereby affecting the initiation and propagation of SCC. As known to all, the passive films formed on the surfaces of SSs play a vital role in their corrosion processes of SSs, and matter their corrosion performances[6]. The composition, structure and properties of the passive films formed the surfaces of

SSs in high temperature water have been studied extensively, showing that the passive films have a double-layer structure with an outer loose layer comprised of iron oxides and an inner compact layer composed of chromium oxides[7-11]. However, the protection and dissolution mechanism of passive film seems controversial, making the studies on the composition, structure and properties of passive films in PWR environments necessary[12-13]. On the other hand, chloride might be involved in the corrosion and stress corrosion cracking behaviors of SSs by changing the structure and properties of passive films. But it was still unclear that the roles of chloride ion in the transition of the corrosion behavior of SSs from passivation to activation[14-16]. Electrochemical impedance spectroscopy (EIS) was used to study the effect of Cl^- concentration on the film-forming behavior of the Z2CND18-12N SS in acidic solutions which was conducted by Boissy[17], but the roles of chloride involved were still unsolved and in debate. Thus, in the electrochemical corrosion process of the Z2CND18-12N SS in high temperature and pressure water[18], it is necessary to conduct more studies to investigate the effect of Cl^- and to clarify its roles. In this paper, the effect of Cl^- on the corrosion behavior of the Z2CND18-12N SS was studied using a series of electrochemical methods, including potentiodynamic polarization, EIS and current-time transient measurements and its roles involved was discussed.

2. MATERIALS AND EXPERIMENTAL PROCEDURES

The chemical composition (in wt.%) of the Z2CND18-12N SS studied in present work is listed in Table 1. A typical microstructure consisted of austenite grains and a number of crystal twins was observed on the etched surface of Z2CND18-12N SS, as shown in Fig. 1. Before tests, the Z2CND18-12N SS samples were cut to cuboid blocks of 3cm^2 exposed surface areas, grounded with sand paper to 1200#, cleaned with mixed liquor of acetone, analytically pure alcohol and methylbenzene (1:1:1, vol.%) and finally dried using cold air.

Table 1. Chemical composition of the Z2CND18-12N SS in present work (in wt.%).

C	Si	Mn	P	S	Mo	Cr	Ni	Co	Nb	N	Fe
0.0130	0.491	1.800	0.0090	0.0032	2.23	18.52	11.96	0.0330	0.0080	0.032	Balanced

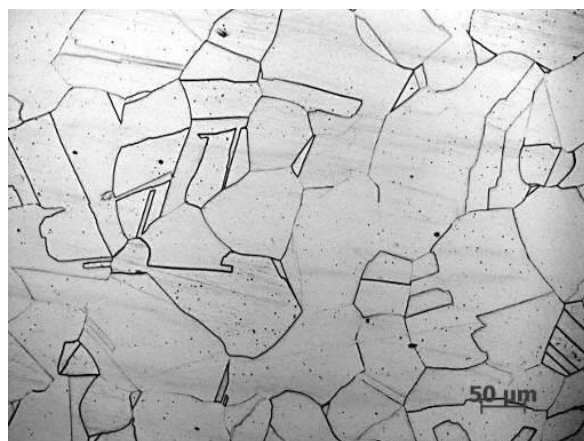


Figure 1. Microstructure of the Z2CND18-12N SS.

The experiments were conducted in an autoclave containing 5 L high temperature high pressure (HTHP) water and the experimental conditions were simulated the water-chemical environments of the primary circuit in PWR nuclear power plants. The concentrations of the HTHP waters were below: 1000 ppmH₃BO₃, 2.2 ppm LiOH, 10 ppm NaCl. The experimental temperature and pressure was 290 °C and 15.4 MPa, respectively. Before heating, the deoxidization was conducted by the continuous purging of 1 MPa argon gas for 2 h.

All electrochemical measurements were carried out in a standard three-electrode cell, in which a large platinum plate was served as the counter electrode, an external pressure balanced Ag/AgCl electrode as reference electrode and the Z2CND18-12N SS as working electrode[19]. The Ag/AgCl reference electrode (reference solution: 0.1 M KCl solution) was placed in a separate compartment sustained at an ambient temperature and system pressure by a solution bridge, which was described in detail elsewhere[20]. All electrode potentials presented in this work have been referred to standard hydrogen electrode (SHE) calculated using the following equation (Equation (1))[21]:

$$E_{SHE} = E_{obs} + 0.2866 - 0.001(T - t) + 1.745 \times 10^{-7}(T - t)^2 - 3.03 \times 10^{-9}(T - t)^3 \quad (1)$$

where E_{SHE} , E_{obs} , T and t stands for the electrode potential of the working electrode (V_{SHE}), its measured electrode potential, the temperature used in the present work and room temperature (298 K), respectively.

The potentiodynamic polarization measurements were performed from -1 V_{SHE} to 1.5 V_{SHE} at a scanning rate of 20 mV/min. The EIS were measured at a constant potential in the passive range in the frequency range from 100 kHz to 0.01 Hz with a ± 5 mV amplitude. Prior to the measurements of potentiodynamic polarization curves and EIS, the samples were cathodically cleaned at -1.5 V_{SHE} for 5 min to reduce air-formed oxides formed on the sample surface, followed by the immersion tests in the given solution to achieve the stabilization of corrosion potentials. In potentiostatic experiments, the variation of current with time (I-t curves) of the electrodes at a fixed potential (0.1 V_{SHE}) was immediately measured after cathodic reduction to obtain the formation information of the passive film. Each electrochemical measurement was repeated at least three times to ensure good data reproducibility.

3. RESULTS AND DISCUSSION

3.1. Potentiodynamic Polarization Plots

Fig. 2 shows the potentiodynamic polarization plots of the Z2CND18-12N SS in three different solutions. As seen from Fig. 2, Z2CND18-12N SS exhibits typical active-passive behavior. The corrosion behaviors of Z2CND18-12N SS are similar but their corrosion potential (E_{corr}) and corrosion current density (i_{corr}) are notably different, and the values of E_{corr} and i_{corr} based on Tafel extrapolation analysis derived from Fig. 2 are listed in Table 2. With the addition of Cl⁻ in the solution, the E_{corr} and i_{corr} of the sample gradually shifted positively. At the same time, when the Cl⁻ in the solution changed from zero to 10ppm, the E_{corr} positively shifted from -505 mV_{SHE} to -445 mV_{SHE} and the i_{corr} increased

4 times, while the total Cl^- in the solution increased again (10ppm to 100ppm), although both E_{corr} and i_{corr} have increased, but the change is not significant. In addition, all curves show significant passivation behavior, although the sample has three anodic passivation zones in the chloride-free and 10 ppm chloride solutions, and only two passivation zones in the 100 ppm solution. Also, the addition of Cl^- also increased the initiating passive current density (I_{cc}), maintaining passive current density (I_{p}) of the Z2CND18-12N SS and the primary passivation potential, leading to the shrinking of the passive regions.

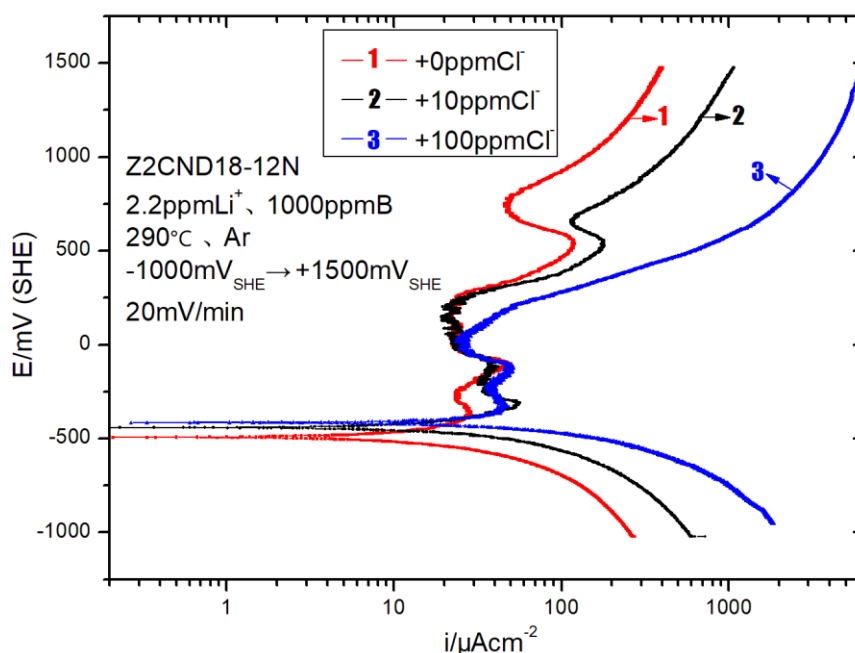


Figure 2. Potentiodynamic polarization plots of the Z2CND18-12N SS in B-Li HTHP water with or without Cl^-

Table 2. Fitted parameters from the potentiodynamic polarization plots in Fig. 2.

Solution	$E_{\text{corr}}/\text{V}(\text{vs SHE})$	$i_{\text{corr}}/\text{A}\cdot\text{cm}^{-2}$
1000ppmB+2.2 ppmLi+100ppm Cl^-	-0.430	3.13×10^{-5}
1000ppmB+2.2 ppmLi+10ppm Cl^-	-0.445	2.21×10^{-5}
1000ppmB+2.2ppmLi	-0.505	5.27×10^{-6}

Yang[22] claimed that the Cl^- could compete with the oxidizing substances in the passive films and even could result in substitution of metal chlorides in the passive films, which induced a certain amount of lattice defects generated and eventually decreased the electrical resistivity of the passive films. This made it difficult to sustain passivation in water environments containing Cl^- . From Figure 2, it was also found that the corrosion current density fluctuated greatly between the primary and secondary passive regions in the tested solution containing 10 ppm and 100 ppm Cl^- , indicating that Cl^- could lower the stability of the passive films and lead to the breakdown and re-deposition of the films alternately[23].

It can be attributed to involvement of Cl^- in the corrosion films, raising the differences of electrode potentials between the activated and passivated areas covered with the corrosion films, which satisfied the thermodynamic conditions of electrochemical corrosion[24]. During the electrochemical corrosion process, the activated and passivated areas acted as anode and cathode respectively, and the former was only a little area while the latter was large in this situation, making the achievement of large cathode and small anode. Consequently, the corrosion rates and currents of the anodes were much larger than the cathodes, leading to the breakdown of local passive film. This is why the both the primary and secondary passive regions became narrower and the passive film was less stable[25].

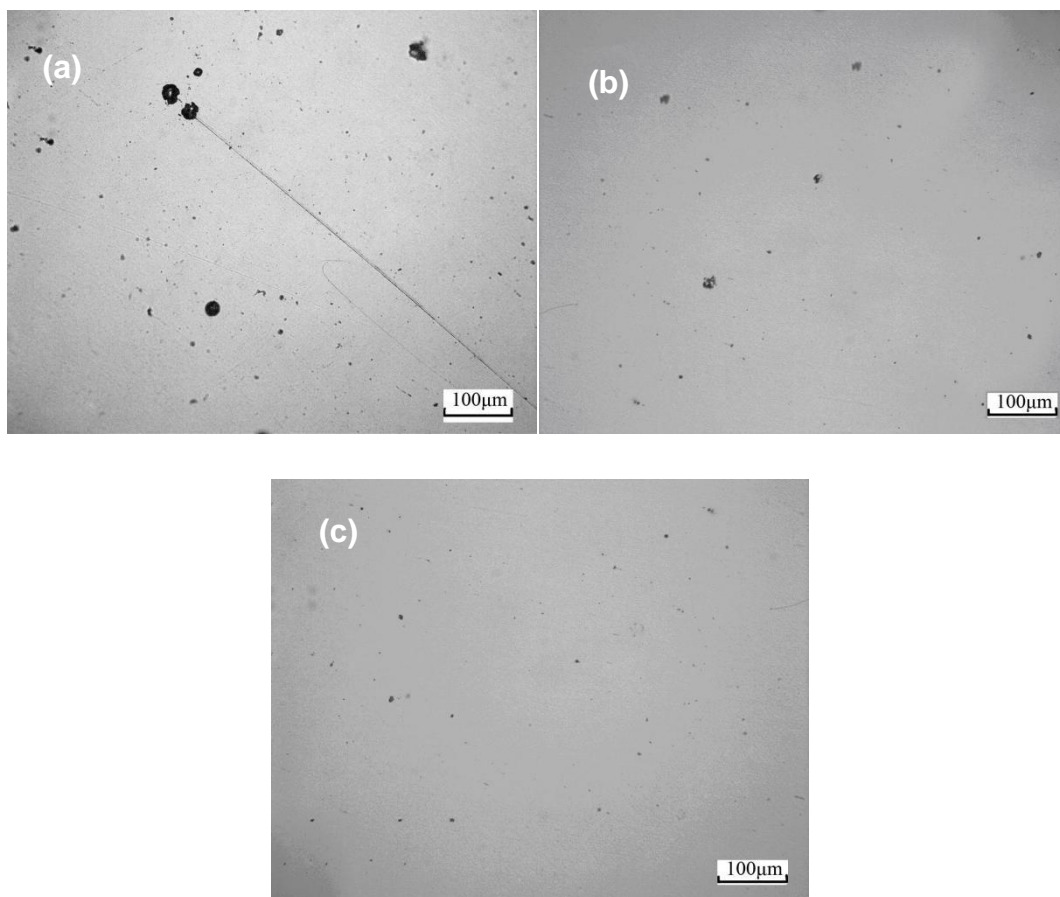


Figure 3. Micro-topography photo of the sample surface after the polarization test. (a)1000ppmB + 2.2 ppmLi + 100ppm Cl^- (b)1000ppmB + 2.2 ppmLi + 10ppm Cl^- (c)1000ppmB + 2.2ppmLi.

Further observation of the micro-topography photo of the sample surface after the polarization test shows that: in the corrosive medium containing Cl^- , Fig. 3(a)(b), the observed pits are large, and their shape is irregular; in the medium containing B and Li^+ but no Cl^- , the pitting corrosion is also observed and pits on the sample surface are small and few, Fig. 3(c). The oxide films formed on the surface of the stainless steel in the high-temperature water containing B and Li^+ have a double-layer structure[6]. The near surface layer is oxide with a higher oxygen content[8], and the inner layer is oxides with a lower oxygen content. These oxides are different from the stainless steel substrate with face-centered structure, making the presence of an interface between the oxide film and the stainless steel

substrate. At the same time, during the growth of the oxide films, it mainly depends on the migration of metal cations from the substrate and the anions from the outside[26]. The rate of metal cation migration is very low, leading to the formation of a lot of vacancies at the interface between stainless steel matrix and the oxide films, while the growth of the oxide films caused the accumulation of defects at the interface, which might lead to the shrink of oxide films to the surface[27]. But the oxide film tends to hinder the shrinkage process, which may generate an additional tensile stress on the aforementioned interface. If a small amount of active anion like Cl^- is added to the corrosive medium, the oxide film structure will be changed and its porosity might increase, which favors the growth of the oxide film and thus makes the above additional tensile stress greater and cause the concentration of local stress[28]. At these areas, it is easier to initiate pitting corrosion, which increases the sensitivity of localized corrosion[29-30].

3.2. Electrochemical Impedance Spectroscopy

Fig. 4 shows the EIS spectra of the Z2CND18-12N SS in the tested solutions. The shapes of impedance spectra obtained in two solutions were similar, which presented as a single capacitive reactance arc.

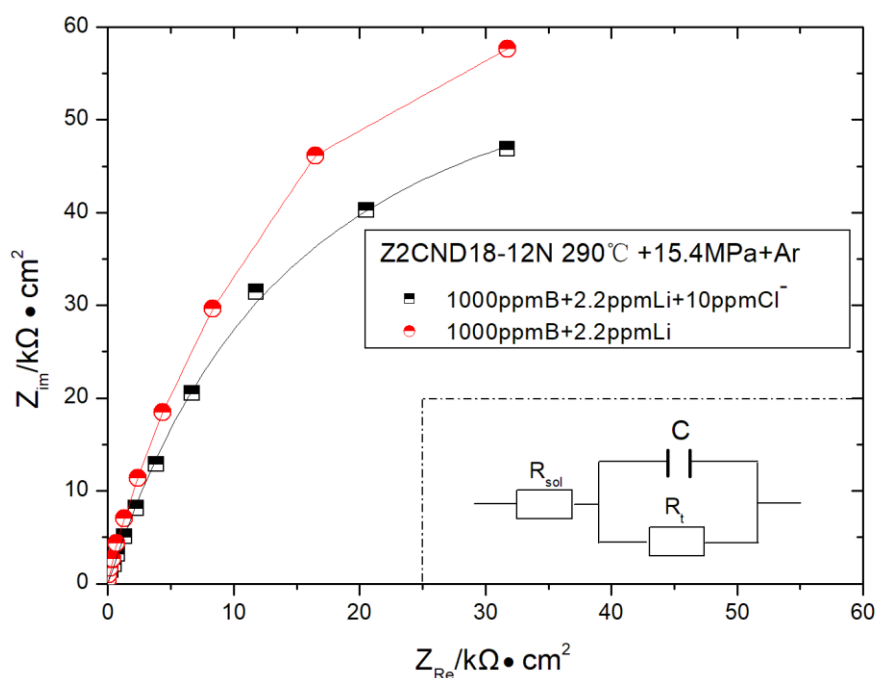


Figure 4. EIS spectra of the Z2CND18-12N SS in B-Li HTHP water with or without Cl^-

The value of capacitance in experimental solution without Cl^- was higher than that containing 10ppm Cl^- , suggesting that the protectiveness of the films formed was much better[17]. Table 3 showed the analyzed results of the resistance of the solution (R_{sol}), double layer capacitance (C) and charge transfer resistance (R_t) in both solutions fitted from the impedance spectra in Fig. 4. The value of R_t of

passive film formed in solution without Cl^- was also much larger[31], which means the charge on the surface of the tested materials was more difficult to transfer and corrosion resistance of the film was better[32]. These results were consistent with those obtained from analyses of the polarization curves[33] (in Table. 2).

Table 2. EIS fitting results from the Fig. 4 (R_{sol} : Resistance of the solution, R_t : charge transfer resistance, C: double layer capacitance).

Solution	$R_{\text{sol}}/\Omega \cdot \text{cm}^2$	$C/\text{F} \cdot \text{cm}^{-2}$	$R_t/\Omega \cdot \text{cm}^2$
1000ppmB+2.2 ppm Li	10.27	4.18×10^{-5}	2.21×10^5
1000ppmB+2.2ppmLi+10ppm Cl^-	8.75	3.75×10^{-5}	1.76×10^5

3.3. I-t Curves

Fig. 5 shows the I-t transient curves of the Z2CND18-12N SS in two different kinds of solutions. Before tests, the samples were polarized at $-1.5 \text{ V}_{\text{SHE}}$ for 300 s to obtain a fresh surface, and then anodically polarized at $0.1 \text{ V}_{\text{SHE}}$ to form the passive film. In both conditions, the nucleation and growth of the films on the surfaces were much quicker than their decomposition at the beginning, making the corrosion current density rapidly decreasing. The corrosion current density did not tend to be stable until a layer of passive films were formed on the surfaces.

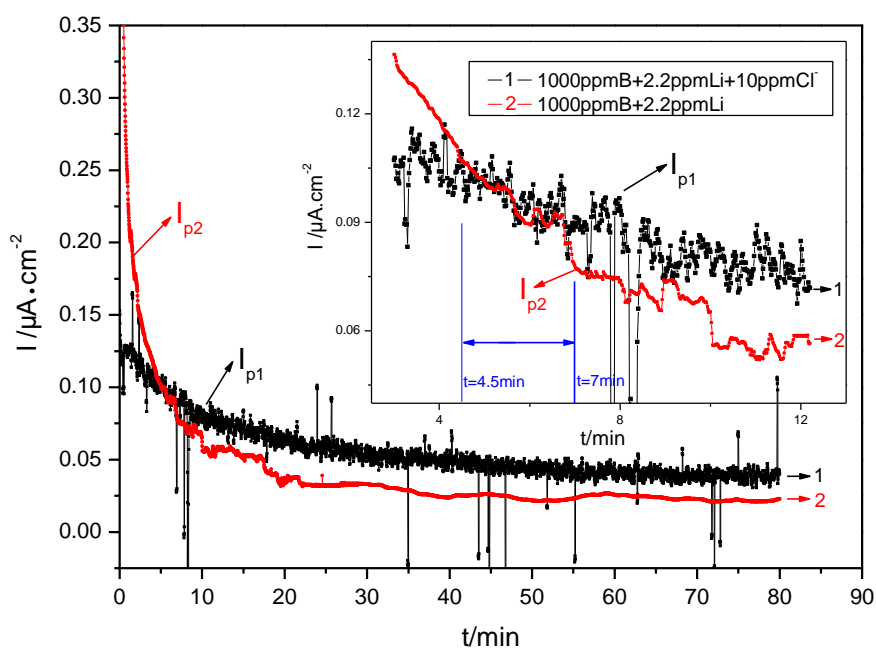


Figure 5. Potentiostatic curves of Z2CND18-12N SS in HTHP B-Li water with or without Cl^-

When the time was less than 4.5 minutes, the I_{p1} obtained in B-Li HTHP water in the presence of Cl^- was less than the I_{p2} obtained in B-Li HTHP water in the absence of Cl^- , especially at early beginning of tests. The corrosion current densities in B-Li HTHP water containing 10ppm Cl^- (I_{p1}) and without Cl^- (I_{p2}) were almost the same during the time was between 4.5 and 7 minutes. However, the I_{p1} was exceeded the I_{p2} when the time was > 7 minutes. It indicated that the corrosion rate in B-Li HTHP water in the absence of Cl^- was higher at the beginning of the tests, and became lower at the subsequent period of the tests. This can be attributed to the damage effect of the Cl^- during the dynamic balance of dissolution and repairing of the passive film before the new balance was reached[34-35]. The presence of more frequently-fluctuated corrosion current in the I-t curves suggested that the stability of the passive film in B-Li HTHP water containing 10 ppm Cl^- was lower. Marcus[36] believed that the Cl^- can absorb on the surface of passive film preferentially, exclude the adsorbed oxygen, combine with metal cations to produce dissoluble chlorides, leading to Cl^- induced film breakdown.

After cathodic cleaning to reduce the air-formed oxides, the electrodes were polarized at a given potential in the passive region in Fig. 2 to measure the variation of current (I) with time (t). The measured current was found to decrease with the increase of the time according to Equation (2)[37-38]:

$$\log I = \log A + k \log t \tag{2}$$

in which k and A represents the slope of the double-log potentiostatic polarization plot and the constant related to the applied potential, respectively. According to Lakatos et al.[35], $k = -1$ yields the formation of a compact and protective oxide, while $k = -0.5$ suggests the formation of a less-protective oxide with a fair amount of defects and its growth proceeding via as a dissolution and deposition process. When the k value is closer to 0, the oxides became more shrinkage.

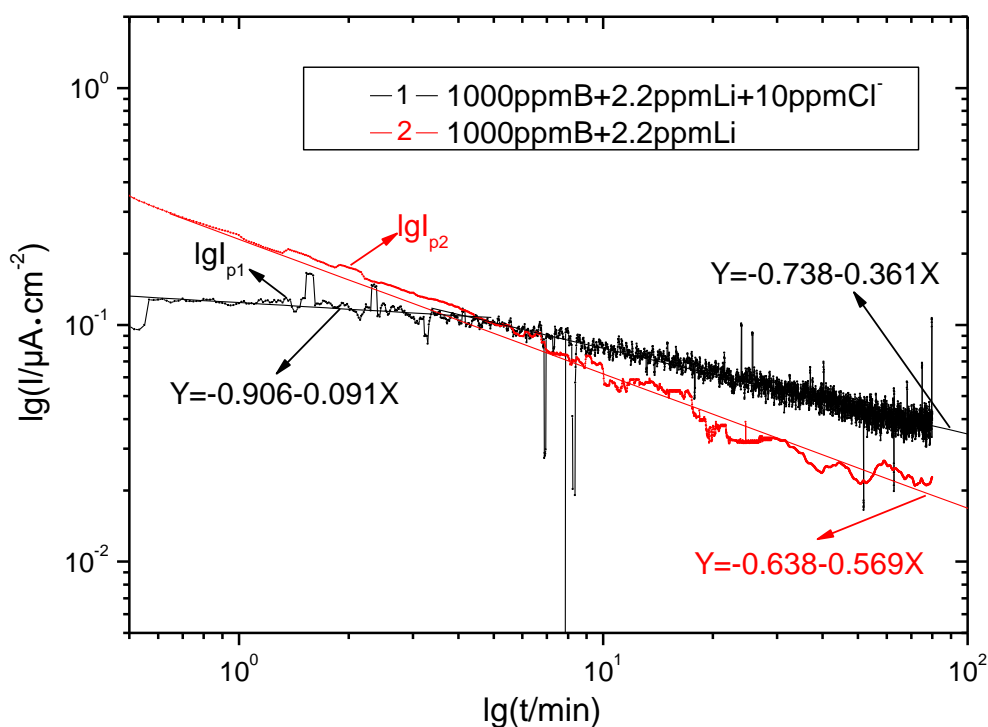


Figure 6. Current-time transient curves of the Z2CND18-12N SS at 0.1 V_{SHE} in B-Li HTHP water with or without Cl^-

Fig. 6 shows the double-log potentiostatic polarization plots at $0.1V_{SHE}$ in the two solutions. In B-Li HTHP water in the absence of Cl^- , k was equal to -0.569 . And the value of k in B-Li HTHP water containing 10 ppm Cl^- changed from -0.091 to -0.361 , suggesting that a loose passive film with a high amount of defects formed at the beginning and became denser with the increase of time[39]. These k values were much larger than -1 , which indicates that there were plentiful defects present in the passive films formed in these two solutions.

In the passive region, the slope value of current-time transient curve (i.e., Fig. 6) can directly reflect the protectability of the passive films formed on the surface of the studied material. At a given potential where the sample was passivated, the anion/cation exchange and the deposition of the passive film formed at the interface of oxide/solution were at a relatively dynamic balance. Under these circumstances, the rate-determining step of the corrosion process was the transfer process of the anion or cation involved, and the amount of the anion or cation diffusing/migrating through the passive film per unit time was proportional to the corrosion current density of the passivation process. As mentioned previously, Cl^- can destroy the dynamic balance of dissolution and repassivation processes and accelerate the dissolution of the passive film when the applied potential was $0.1V_{SHE}$ and the time was less than 4.5 min. The process would inevitably compete against the oxygen adsorption at the interface, leading to the decrease of the corrosion current density compared to that in the absence of Cl^- . However, since the Cl^- could complex with metal cations to change the structure and properties of the passive film, it would create more defects in the passive film when the time was > 7 min, which facilitated the transport of cations/anions through the film and accelerated the anodic process. This would make the corrosion current density larger at an extended polarized time, Fig. 6.

4. CONCLUSION

(1) The polarization curves of the Z2CND18-12N SS in B-Li HTHP water showed that it exhibited a wide passive region with three anodic peaks. The addition of Cl^- to B-Li HTHP water positively shifted the corrosion potential, accelerated the corrosion current density and shrank the passive region.

(2) Cl^- was involved in the formation of the passive films on the Z2CND18-12N SS surface in B-Li HTHP water, which changed the structure and property of the passive films by the competition against oxygen adsorption, the complexation with metal cations and the generation of defects accumulated in the passive film. The process eventually led to the deterioration of the protectability and stability of the passive films.

(3) When the polarized time was less than 4.5 minutes, the corrosion current density of the Z2CND18-12N SS in B-Li HTHP water containing 10 ppm Cl^- was lower than that in the absence of Cl^- ; while it turned to be opposite when the time was > 7 min. This was attributed to the change of Cl^- role from adsorption competition to cation complexation.

ACKNOWLEDGMENTS

The authors would like to thank the National Key Research and Development Program of China (No. 2016YFB0700404), Natural Science Foundation of China (No. 51375182) and Major Natural Science Foundation of China (No. U1260201) for their financial support.

References

1. P.P. Joshi, N. Kumar and K.L. Murty, *Encyclopedia of Materials: Metals and Alloys*, 1(2022)364
2. D. Féron, E. Herms and B. Tanguy, *J. Nucl. Mater.*, 427(2012)364
3. U. Ehrnsten, *Comprehensive Nuclear Materials (2nd Edition)*, 4(2020)118
4. M.L. Calvar and I.D.Curières, *Nuclear Corrosion Science and Engineering*, 15(2012)473
5. G.F. Li, Y.F. Yuan and X. Lu, *Procedia Eng.*, 130(2015)1572
6. G. Tranchida, M. Clesi, F. Di Franco, F. Di Quarto and M. Santamaria, *Electrochim. Acta*, 273(2018)412
7. J.J. Chen, Q. Xiao, Z.P. Lu, X.K. Ru, H. Peng, Q. Xiong and H.J. Li, *J. Nucl. Mater.*, 489(2017)137
8. H.B. Lee, J. Chen, S. Meng, C. Jang, S.H. Park, Q. Xiao, H.J. Lee and K.-H. Na, *J. Nucl. Mater.*, 556(2021)153193
9. K. Jaffré, H. Abe, B. Ter-Ovanesian, N. Mary, B. Normand and Y. Watanabe, *J. Nucl. Mater.*, 556(2021)153258
10. Z. Que, C. Huotilainen, T. Seppänen, J. Lydman and U. Ehrnsten, *J. Nucl. Mater.*, 558(2022)153399
11. Q. Xiao, C. Jang, C. Kim, H. Kim, J. Chen and H.B. Lee, *Corros. Sci.*, 177(2020)108991
12. S.K. Pradhan, P. Bhuyan, L.R. Bairi and S. Mandal, *Corros. Sci.*, 180(2021)109187
13. B. Stellwag, *Corros. Sci.*, 40(2)(1998)337
14. D. Du, K. Chen, H. Lu, L. Zhang, X. Shi, X. Xu and P.L. Andresen, *Corros. Sci.*, 110(2016)134
15. D.G. Li, J.D. Wang, D.R. Chen and P. Liang, *J. Power Sources*, 272(2014)448
16. S.M. Elsariti and Haftirman, *Procedia Eng.*, 53(2013)650
17. C. Boissy, C. Alemany-Dumont and B. Normand, *Electrochem. Commun.*, 26(2013)10
18. X. Zhong, M. Li, B. Zhou, M. Yao and J. Shen, *Corros. Sci.*, 182(2021)109223
19. M. Sophocleous and J.K. Atkinson, *Sens. Actuators, A.*, 267(2017)106
20. J.-S. Lee, *J. Electroanal. Chem.*, 859(2020)113872
21. B.W.F. Bogaerts, *Electrochim. Acta*, 212(2016)102
22. I.-J. Yang, *Corros. Sci.*, 33(1) (1992) 25
23. Q. Hou, Z. Liu, C. Li, X. Li and J. Shao, *Appl. Surf. Sci.*, 467-468(2019)1104
24. L. Freire, M.J. Carmezim, M.G.S. Ferreira and M.F. Montemor, *Electrochim. Acta*, 56(14)(2011)5280
25. W. Tian, N. Du, S. Li, S. Chen and Q. Wu, *Corros. Sci.*, 85(2014)372
26. Z. Shen, D. Tweddle, H. Yu, G. He, A. Varambhia, P. Karamched, F. Hofmann, A.J. Wilkinson, M.P. Moody, L. Zhang and S. Lozano-Perez, *Acta Mater.*, 194(2020)321
27. D. Singh, F. Cemin, M.J.M. Jimenez, V. Antunes, F. Alvarez, D. Orlov, C.A. Figueroa and S.S. Hosmani, *Appl. Surf. Sci.*, 581(2022)152437
28. B. Krawczyk, P. Cook, J. Hobbs and D.L. Engelberg, *Corros. Sci.*, 142(2018)93
29. R.P. Matthews, R.D. Knutsen, J.E. Westraadt and T. Couvant, *Corros. Sci.*, 185(2021)109454
30. K.W. Fang, C.T. Li, S. Dong, D.B. Zhang, X.f. Wu and H.X. Hu, *Scanning*, (2021)6661872
31. Y.B. Tang, X.W. Shen, Z.H. Liu, Y.X. Qiao, L.L. Yang, D.H. Lu, J.S. Zou and J. Xu, *Acta Metall. Sinica*, 58(3)(2022)324
32. J. Yang, Z.B. Wang, Y.X. Qiao and Y.G. Zheng, *Corros. Sci.*, 199(2022)110210.
33. Y. Qiao, X. Wang, L. Yang, X. Wang, J. Chen, Z. Wang, H. Zhou, J. Zou and F. Wang, *J. Mater. Sci. Technol.*, 107(2022)197
34. Z. Wang, A. Seyeux, S. Zanna, V. Maurice and P. Marcus, *Electrochim. Acta*, 329(2020)135159
35. I. Díez-Pérez, C. Vericat, P. Gorostiza and F. Sanz, *Electrochem. Commun.*, 8(4)(2006)627
36. P. Marcus and J.M. Herbelin, *Corros. Sci.*, 34(7)(1993)1123

37. N. Li, S. Shi, J. Luo, J. Lu and N. Wang, *Surf. Coat. Technol.*, 309(2017)227

38. M. Lakatos-Varsányi, F. Falkenberg and I. Olefjord, *Electrochim. Acta*, 43(1)(1998)187

39. C.B. Nascimento, U. Donatus, C.T. Ríos and R.A. Antunes, *J. Materi. Res. Technol.*, 9(6)(2020)13879

© 2022 The Authors. Published by ESG (www.electrochemsci.org). This article is an open access article distributed under the terms and conditions of the Creative Commons Attribution license (<http://creativecommons.org/licenses/by/4.0/>).